Predicting Individual Brain MRIs at Any Age Using Style Encoding Generative Adversarial Networks

Shruti Gadewar, Abhinaav Ramesh, Mengting Liu, Iyad Bagari, Talia Nir, Paul Thompson and Neda Jahanshad

October 11, 2022

Predicting individual brain MRIs at any age using style encoding generative adversarial networks

Shruti P. Gadewar*[a], Abhinaav Ramesh[a], Mengting Liu[b], Iyad Ba Gari[a], Talia M. Nir[a], Paul Thompson[a], Neda Jahanshad[a]

[a]Mark and Mary Stevens Neuroimaging and Informatics Institute, University of Southern California, Marina del Rey, CA, 90292, USA;
[b]School of Biomedical Engineering, Sun Yat-sen University, Shenzhen, 518107, China

ABSTRACT

Brain structural changes in older adults over time can help identify and predict which individuals are at risk for neurodegenerative disorders and dementias. These trajectories are traditionally calculated by assessing localized rates of brain tissue atrophy from a longitudinal series of brain MRIs as compared to group averages. However, these methods do not preserve individual differences in brain structure, which may provide added information regarding risk. A map of how an individual's brain may look at a given age - in the case of a normal, healthy, aging trajectory - may help to identify deviations and abnormalities when presented with a true scan at that age. Here, we consider estimating the age-related brain changes as a domain transfer problem. We develop a fully unsupervised generative adversarial network (GAN) with cycle consistency reconstruction losses, trained on cross-sectional brain MRI data from participants of the UK Biobank aged 45 to 81. We show that brain MRIs for males and females at a given age can be predicted by converting the content information encoded in a T1-weighted MRI (i.e., the individual's identifying anatomical features), accompanied by adding the style (age/sex) information from a reference group. Results on the PREVENT-AD cohort demonstrated that our style-encoding domain transfer model can predict follow-up brain MRIs, successfully, without relying on longitudinal data from the subjects. We show how deviations from the predicted images are indicative of factors related to neurodegenerative disease risk.

Keywords: domain transfer, GAN, aging patterns, brain MRI, APOE4

1. INTRODUCTION

The human brain undergoes dynamic structural changes with age[1]. Brain mapping studies often aim to identify the patterns of regional changes that may be indicative of an underlying disease; for example, accelerated temporal lobe atrophy may be indicative of risk for late-onset Alzheimer's disease (AD) and related dementias[2]. Traditional brain mapping approaches often use non-linear registrations between longitudinally collected brain MRIs to calculate local deformations, which are later compared across subjects in a template space[3]. While these efforts are important for understanding group trends, they are susceptible to biases from template selection and creation[4, 5, 6], and often rely on images from subjects scanned across a wide range of intervals, adding scanner and scanner drift variability as confounds. The ability to generate an individual's brain MRI at a given age could help with the detection of more subtle effects, such as the effect of a genetic marker on brain structure. If scans were acquired from individuals all at the same age, then statistical models would not need to include these age-related nuisance variables and may be better powered to study subtle effects[5].

Generated images of future brain MRIs could also suggest how the brain would age under healthy, normal, conditions creating a benchmark for an individual's brain structure at any age. Deviations detected in the true image, as compared to the generated image, could serve as proxies for disease related abnormalities or risk factors for decline, such as being carriers of the major genetic risk factor for AD, APOE4. This concept has been encapsulated in "brainAge", a single metric used to describe the most likely age for an individual based on brain MRI features[7]. However, in addition to losing anatomical specificity, brainAge has several other limitations as detailed in [8]. A generated 3D brain MRI would provide a detailed map of where the deviations occur.

Recently, deep learning-based models have been used in brain MRI generation and synthesis to simulate and predict future neurodegenerative trajectories[9, 10, 11]. Several methods have been proposed to achieve this task. A few implementations combine geodesic regression with deep learning to capture longitudinal brain changes[12]. Early models predicted the brain changes using population-based patterns without considering individual differences[13]. More recent deep generative methods used generative adversarial networks (GAN)[14] or a conditional adversarial autoencoder[11]. Such methods require large amounts of longitudinal data that cover a long-time span with frequent sampling to provide the ground truth to supervise the training, and this data is typically very difficult and expensive to acquire. Other unsupervised methods, such as the conditional variational autoencoder (VAE) and conditional GAN[15] have been used to predict MR images of older individuals from their younger selves using cross-sectional data; yet these models are not currently capable of including informative covariates such as sex. Furthermore, the quality of the images may not be sufficient for downstream automated image processing.

Deep learning methods have also achieved diverse image translations by disentangling the image into 'content' and 'style' spaces[16], where contents represent low level information in images such as contours and orientations, and styles can be considered high level information such as colors and textures. Images from different domains share the same content space but show different styles. This breakdown has been applied to show promising results for MRI harmonization[17, 18], and cross-modality medical image conversions[19].

We consider the aging brain prediction as a domain transfer problem rather than a conditional image synthesis problem, where the individual anatomic patterns (or contents) from MR images collected from different ages (styles) belong to different domains but share the same latent content space, and can be converted between each other. These content patterns, which reveal the individually different brain anatomical structures, can be learned using an unsupervised cycle consistent GAN model. Thus, no longitudinal images are needed from the same subjects. Here we describe our model and its implementation, and we compare our results with a framework based on the conditional adversarial autoencoder (CAAE) that was originally used for face aging applications. We highlight our results on an independent test set with longitudinal validation data, showing that our generated images can indeed pick-up age related trends, and can be used as inputs for widely-available automated neuroimage data processing tools to generate features that are sensitive to risk factors for neurodegeneration, specifically APOE4.

2. METHODS

2.1 The architecture of the style-encoding GAN

We used the single StarGAN-v2 framework[20], which consists of a single encoder E, generator G, and discriminator D (**Figure 1**). We consider X to be a set of brain MR images and Y the set of age and sex specific domains; across five year age bins between the ages of 45 and 80, we had 14 domains - seven each for males and females. Given an image $x \in X$ and the original age bin $y \in Y$, we trained this network to produce output images in all the age domains for the subject's indicated sex. The style encoding block E was designed to extract the age information to produce age/sex specific styles using training images binned into the various domains. This allows G to translate an input image x into an output image $G(x,t)$ to reflect the aging pattern of the target age bin y_t. Here, $t = M(z,y_t)$ is the age factor for input x, generated using a mapping network M from sampling a latent vector z and the target domain y_t. The target age group t is then associated with both the target domain patterns as well as the domain-irrelevant patterns from the input image. t, rather than z, is used because the intermediate latent space obtained from the mapping network does not have to support sampling of the latent vector z according to a fixed distribution, thus enforcing a disentangled representation to generate more realistic images[21]. Adaptive instance normalization (AdIN)[22] was used to inject t into G. The discriminator D then tries to distinguish between the original input image x and the generated output image $G(x,t)$ produced by G. The network trains E such that if an image was generated based on age bin t, then t would also be encoded when this generated image is an input to E with the target domain: $E(G(x, t), y_t) = t$.

2.2 Network Losses

Our model was trained using the following losses:
Adversarial loss. Generator G produces $G(x, s)$ where x is the input image and s is the target style code $M(z, y)$. This target style code is generated while training the network, where M is the mapping network and z is a random latent code. The discriminator D tries to distinguish the output image $G(x, s)$ from the input image using the adversarial loss shown below:

$$L_{GAN} = E_x[logD(x)] + E_{x,z}[log(1 - D(G(x, s)))]$$

Cycle-consistency loss[23]**.** This term is the difference between input and the generated images. This loss is used to check if the generated images preserve the anatomical patterns of the input image x:

$$L_{cyc} = E_{x,z}[\|x - G(G(x,s), s_x)\|_1]$$

where $s_x = E(x, y)$ is the estimated style code of the input image x. The generator G learns to preserve the characteristics of input image x and incorporate the style s_x.

Style reconstruction loss. This loss enforces the generator G to use the style code s from a reference set to produce an output image $G(x, s)$ with the encoder:

$$L_{sty} = E_{x,z}[\|s - E(G(x,s))\|_1]$$

Style diversification loss[24]**.** This regularizes the generator G to explore the image space and generate diverse images to preserve the individuality of each input image:

$$L_{div} = E_{x,z_1,z_2}[\|G(x,s_1) - G(x,s_2)\|_1],$$

where s_1 and s_2 are the target style codes generated using the mapping network M and two random latent codes z_1 and z_2 (i.e., $s_i = M(z_i)$ for i $\in$ {1, 2}).

Complete loss. Combining all the losses together - with λ_{cyc}, λ_{sty} and λ_{div}, being the hyperparameters for each of the losses - the final objective function is:

$$L(G, M, E, D) = L_{GAN} + \lambda_{cyc}L_{cyc} + \lambda_{sty}L_{sty} - \lambda_{div}L_{div}$$

Fig 1. A. The architecture of the style-encoding GAN. Generators learn to generate images by inputting a source image and a style code (age pattern). The learning process is guided by an adversarial loss, cycle consistency loss, and a style reconstruction loss. **B.** The detailed architecture of the generator in the network. In each block, the three numbers represent the number of input channels, output channels, and the image size, respectively.

2.3   2D implementation on 3D images

Our model is based on a PyTorch implementation of StarGANv2 (https://github.com/clovaai/stargan-v2.git). The model was trained on one GPU node on a Cisco C480 ML server with 8 SXM2 V100 32 GB, NVLink interconnect and 2 x 6140 Intel Skylake processor for 130,000 epochs for 6 days with a batch size of 4 and the following lambda values: λ_{cyc} =3, λ_{sty} = 2 and λ_{div} = 2. The lambdas were modified until we could see anatomical variability across subjects in the generated images.

Although brain MRI scans are 3D volumes, GPU memory limitations prompted our network architecture to be designed for 2D images instead. We transformed the 3D scan into a series of 3-slice or 3-channel images across the brain's sagittal plane and saved them as conventional PNGs where each channel represented one slice. The model was trained on these PNG images and then the predicted 3 channel image series was stacked and transformed back into a 3D volume.

In the generative adversarial architecture for style transfer, all slices are loaded in such a way that the model learns the transformation across all bins for that particular slice number across each pair of age bins. If an image has to be transformed from age bin 60 to age bin 70, one subject in age bin 70 would be the reference subject and images in age bin 60 will be transformed to age bin 70 using the trained generator. The error in the prediction would be controlled in training by the discriminator; the generator weights are updated to minimize the distance to the desired target population.

2.4   Data Processing

We used a subset of 3,400 T1-weighted brain MR images (age range 45-81) from the UK Biobank dataset[25] which was further split into 2,800 training images (1,400 for each sex) and the rest were used in the validation set. The data distribution is shown in **Table 1**. These subjects were then divided into 5-year age bins to predict the aging patterns more accurately. There were exactly 200 subject images in each age group per sex. All the images were non-uniformity corrected, skull-stripped using HD-BET[26], linearly registered to the MNI template using FSL's *flirt*[27] with 9 degrees-of-freedom and resized to 256×256×256. An independent longitudinal test set of 50 subjects from PREVENT-AD[28, 29] was used for testing the performance of the model. This test set contained images with a 4 year time interval between scans, which fell into distinct age bins. The generated images for each subject were then subjected to two standard image processing pipelines to demonstrate the downstream utility of the generated images. We extracted cortical gray matter volumes using FSL's *fast*[30] and hippocampal volumes using Hippodeep[31].

Table 1. Demographic breakdown of subjects in the two datasets used.

Dataset	Age (years)	N Male/Female	N APOE4 0/1	N Train/Test
UK Biobank	62.5 ± 9.6 (45-81)	1700/1700	2563/837	2800/600
PREVENT-AD	66 ± 4.2 (55-74)	16/34	29/21	0/50

2.5   Statistical analysis

We compared predicted vs original gray matter atrophy rates between APOE4 carriers and non-carriers within PREVENT-AD, adjusting for sex and baseline age. As our GAN is trained on neurologically healthy non-demented individuals from the general population where the large majority of the population does not carry the APOE4 allele, we would expect the difference between the predicted and actual follow-up volumes, as a fraction of the baseline volume, to be larger (i.e., less accurate predictions) for individuals at heightened risk for disease.

### 2.6   Comparison with the Face Aging network model

A conditional adversarial autoencoder (CAAE)[32] based on (https://github.com/ZZUTK/Face-Aging-CAAE.git) was trained on a subset of UK Biobank data (9,851 males, 11,536 females , age : 62±7 years). All the subjects were skull stripped using HD-BET[26], linearly registered with 9 degrees of freedom to the MNI152 space using the FSL's *flirt*[27] command. This model is based on 2D images. Before embarking on a 3-slice sequential sagittal model for a full 3D brain MRI, we initiated model training and comparisons on the mid-axial slice because ventricular regions across different age groups were most evident in this slice. This model was trained for 1000 epochs using the following

hyperparameters: batch size: 100; learning rate: 1×10^{-5}; weight decay: $1\times10e^{-5}$; β_1: 0.9; latent (Z) vector: 200 components on one GPU node on a Cisco C480 ML server with 8 SXM2 V100 32 GB, NVLink interconnect and 2 x 6140 Intel Skylake processor for 4 days.

3. RESULTS

3.1 Qualitative visualizations of the aging brain

Qualitative visualizations of generated images are shown in **Figure 2** alongside true baseline and follow-up scans for a single control male subject from the independent PREVENT-AD cohort. We also highlight successful downstream processing of the generated images by showing the hippocampal segmentation masks and gray matter outlines for all original and generated images. **Figure 3** plots volumes for predicted and original average of left and right hippocampi for baselines and followup.
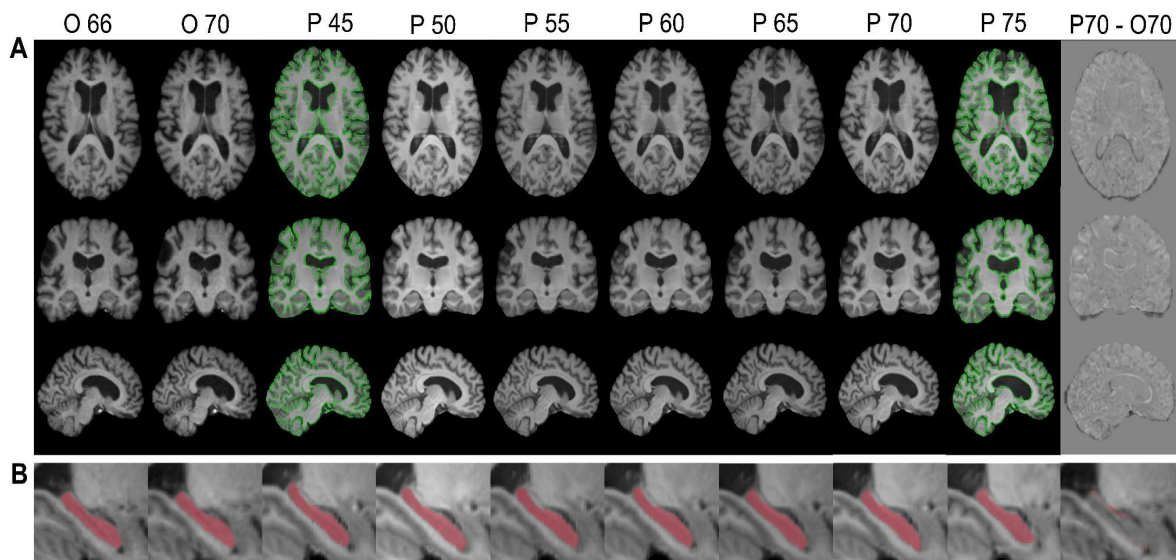
Fig 2. A. Brain age progression- Original "O" axial, coronal and sagittal slices of an input male subject (control) from PREVENT-AD at age 66 and 70 and predictions (P) for the same individual aged 45-49 to 75-80 in five year increments. Changes in areas of CSF (ventricle size) with age are visible. Gray matter masks for the first (P 45) and the last age bin (P 75) have been highlighted in green to highlight successful downstream processing of the generated images. Last column shows the residual image (P70 - O70). **B.** Zoomed in sagittal view of right hippocampal masks extracted on original and generated images indicate the atrophy detected in the hippocampi with respect to age.

3.2 Hippocampal and cortical gray matter volume extractions

For each test subject, the differences between the gray matter volumes for true and predicted follow-up scans were calculated. **Figure 4** highlights the difference between APOE4 carriers and non-carriers. APOE4 status was associated with a greater difference in predicted vs true gray matter volume atrophy rates (p=0.018, se=0.011, β=0.028). Sex was also significant in the model with females having larger volume differences than males (p=0.013, se=0.012, β=-0.033). When we stratified by sex, only females showed significant APOE4 carrier associations with the atrophy predictions (p=0.013, se=0.013, β=0.034).
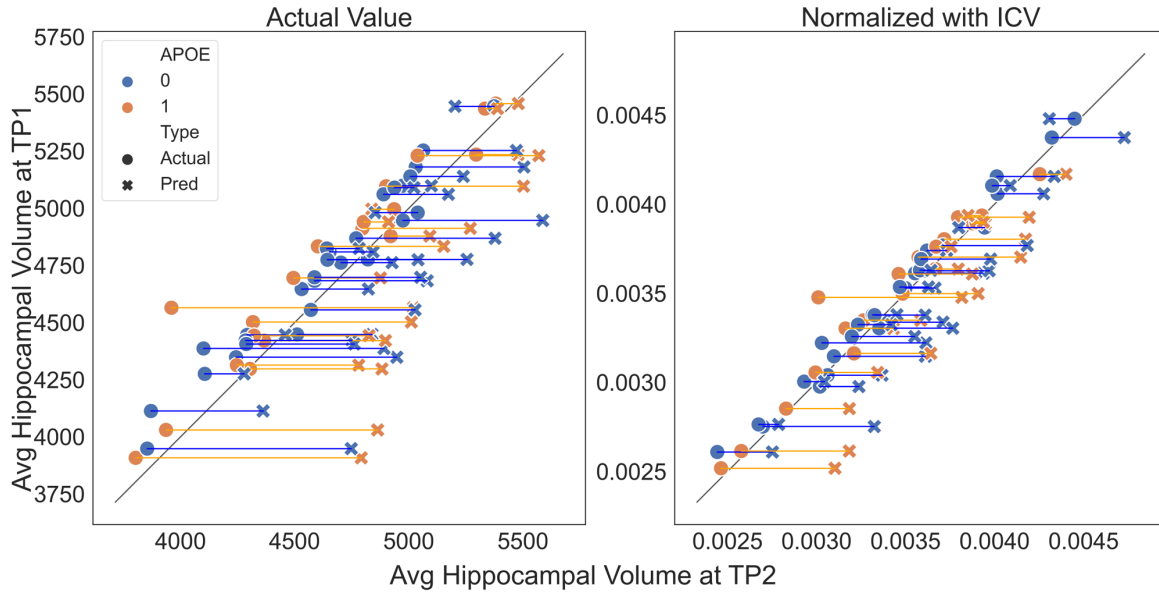
Fig 3. Observed (circle) and predicted (cross) follow-up hippocampal volumes are plotted against the observed baseline volumes for each individual test subject in PREVENT-AD, a cohort of individuals at high-risk for dementia.. *Left:* the observed value of the hippocampal volumes extracted using HippoDeep. *Right:* average hippocampal volumes as a fraction of baseline intracranial volume (ICV). APOE4 carriers are marked in orange, non-carriers in blue. Marks off the lower diagonal of the y=x line indicate larger volumes, while marks on the upper diagonal indicate smaller volumes than baseline. Our model generated images that largely predicted larger volumes than those that were ultimately observed.
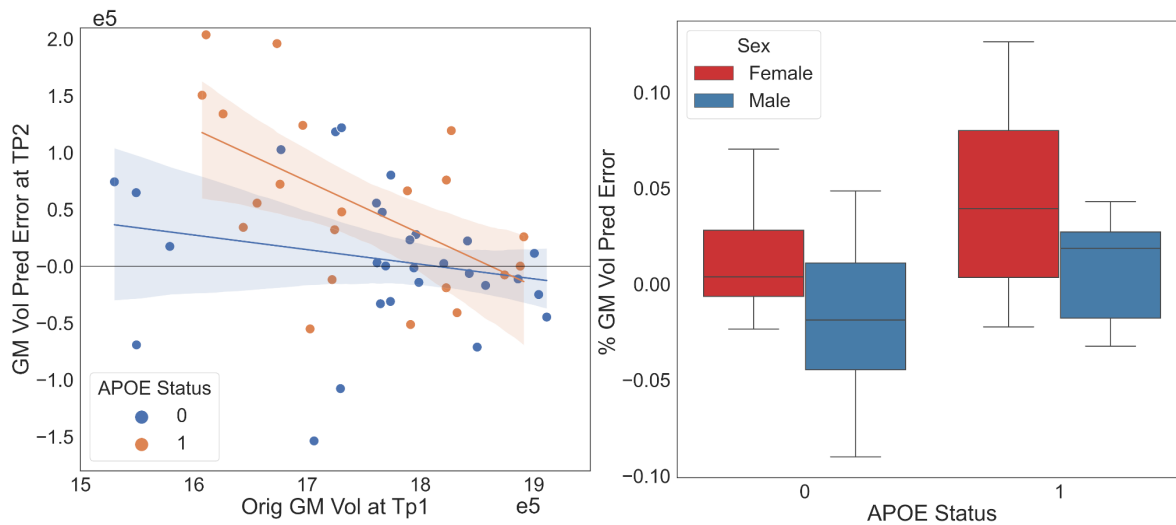
Fig 4. *Left:* A scatter plot of the data shows the differences between the predicted follow-up volumes (Pred Tp2) and the original (observed) follow-up volumes (Orig Tp2) as a function of the original (observed) baseline volumes (Orig Tp1). APOE4 status was associated with the difference in predicted vs true gray matter volume atrophy rates (p=0.018, se=0.011, β=0.028). As our aging model was based on aging without dementia, the error between the predicted and true follow-up scans was found to be higher in individuals at heightened risk for AD, specifically APOE4 carriers than the non-carriers, indicating the error in prediction may serve as a biomarker for diseases. *Right:* Box plots show that female carriers show larger errors between the predicted and observed gray matter volumes after adjustments for baseline gray matter volumes in test data. Females showed significant APOE4 carrier effects (p=0.013, se=0.013, β=0.034), but not males p=0.485.

O 66   P 45   P 50   P 55   P 60   P 65   P 70   P 75   P 80

O 62
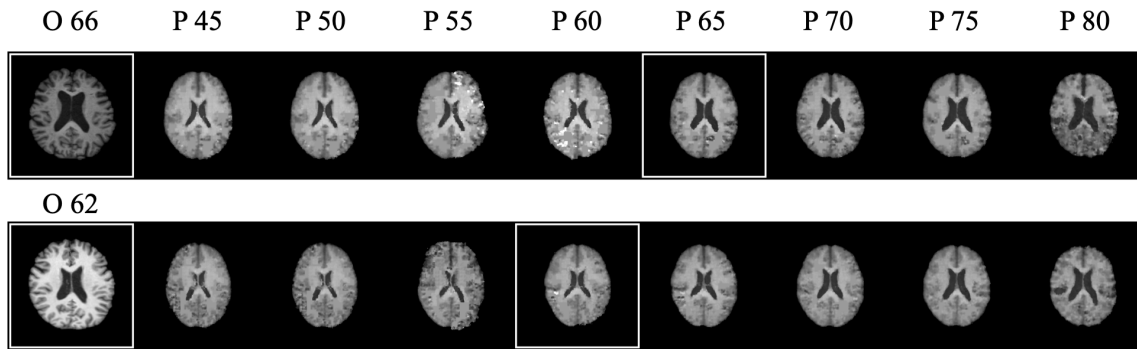
Fig 5. Brain age progression using the CAAE- Observed "O" axial brain MRI slice of input subjects from PREVENT-AD of a male at age 66 years (first row) and a female aged 62 years (second row) respectively; predictions for the same individual aged 45-49 to 80-85 in five year increments. The first white box indicates the original baseline image while the second box shows the model-generated image with an age group closest to the original. Although ventricular enlargement is evident with progressively older age bins, the individuality of the subjects were not preserved and subjects largely resemble each other within specific bins.

4. DISCUSSION AND CONCLUSION

We have shown that domain and style-encoding GANs trained on large cross-sectional MR databases may provide an opportunity to predict how an individual's brain may change under normal, healthy, circumstances, from a single input image at arbitrary age. Our model does not rely on longitudinal images from the same subjects. In comparison with other paradigms, a CAAE model based on FaceAging algorithms (2D color images) also does not rely on longitudinal images and takes less time to train than our current model, but produces similar output for all the inputs. The CAAE model was trained on mid-axial slices, so the ventricular enlargement over a period of time was captured by the model -- yet individual variations were not captured. The output was similar for all the subjects, therefore, only qualitative comparisons were made with the original images. There have also been other implementations to generate 3D brain volumes using cross-sectional data. For example, one line of work aims to generate MRIs for data augmentation purposes using auto-encoding GANs and are not designed to be true to any individual so cannot be used for individualized predictions[33]. Another line of work aims to predict older brain MR images from younger ones using cross-sectional data, but their conditional GAN based model used is not capable of including more covariates such as sex[15].

The proposed style-GAN method described in this work may have several advantages for the neuroscience and aging research communities. A model trained on healthy subjects, such as ours, may also provide a way to set up individual normative models. Such models can monitor the deviation of individual brain changes according to the normative trajectories, which might be more sensitive to track the early progression of abnormalities due to brain diseases. Our work may be viewed as complementary to the common "brainAge" metric, which provides a cross sectional look into whether a brain MRI overall is considered to reflect accelerated aging[7]. Several studies have tried to train deep learning models to predict brain changes conditioned not only on ages but also other clinical information, e.g., white matter hyperintensities[9]. In future work, we will expand our training models to condition aging on more factors, including APOE4 carrier status as a genetic risk for dementia.

ACKNOWLEDGEMENTS

REFERENCES

[1]   Fjell, Anders M., and Kristine B. Walhovd., "Structural brain changes in aging: courses, causes and cognitive consequences." Reviews in Neurosciences, 21.3: 187-222 (2010).

[2]   Rabinovici, Gil D. "Late-onset Alzheimer disease.," Continuum: Lifelong Learning in Neurology 25.1: 14 (2019).

[3]   Hua, X., Ching, C. R., Mezher, A., Gutman, B. A., Hibar, D. P., Bhatt, P., ... & Alzheimer's Disease Neuroimaging Initiative, "MRI-based brain atrophy rates in ADNI phase 2: acceleration and enrichment considerations for clinical trials", Neurobiology of aging, 37, 26-37 (2016).

[4]   Dey, N., Ren, M., Dalca, A. V., & Gerig, G., "Generative adversarial registration for improved conditional deformable templates", ICCV, pp. 3929-3941 (2021).

[5]   Zhu, A. H., Thompson, P. M., & Jahanshad, N., "Age-Related Heterochronicity Of Brain Morphometry May Bias Voxelwise Findings", In 2021 IEEE 18th ISBI, pp. 836-839 (2021).

[6]   Fonov, V., Evans, A. C., Botteron, K., Almli, C. R., McKinstry, R. C., Collins, D. L., & Brain Development Cooperative Group., "Unbiased average age-appropriate atlases for pediatric studies", Neuroimage, 54(1), 313-32 (2011).

[7]   Cole, J. H., & Franke, K., "Predicting age using neuroimaging: innovative brain ageing biomarkers", Trends in neurosciences, 40(12), 681-690 (2017).

[8]   Butler, E. R., Chen, A., Ramadan, R., Le, T. T., Ruparel, K., Moore, T. M., ... & Shinohara, R. T., "Pitfalls in brain age analyses", Vol. 42, No. 13, pp. 4092-4101, Hoboken, USA: John Wiley & Sons, Inc. (2021).

[9]   Rachmadi, M. F., Valdés-Hernández, M. D. C., Makin, S., Wardlaw, J., & Komura, T., "Automatic spatial estimation of white matter hyperintensities evolution in brain MRI using disease evolution predictor deep neural networks", Medical image analysis, 63, 101712 (2020).

[10]   Rachmadi, M. F., C Valdés-Hernández, M. D., Makin, S., Wardlaw, J. M., & Komura, T., "Predicting the evolution of white matter Hyperintensities in brain MRI using generative adversarial networks and irregularity map", In MICCAI, pp. 146-154 (2019).

[11]   Ravi, D., Alexander, D. C., Oxtoby, N. P., & Alzheimer's Disease Neuroimaging Initiative., "Degenerative adversarial neuroimage nets: generating images that mimic disease progression", In MICCAI, pp. 164-172 (2019).

[12]   Ding, Z., Fleishman, G., Yang, X., Thompson, P., Kwitt, R., Niethammer, M., & Alzheimer's Disease Neuroimaging Initiative., "Fast predictive simple geodesic regression. Medical image analysis", 56, 193-209, (2019).

[13]   Sivera, R., Delingette, H., Lorenzi, M., Pennec, X., Ayache, N., & Alzheimer's Disease Neuroimaging Initiative., "A model of brain morphological changes related to aging and Alzheimer's disease from cross-sectional assessments", NeuroImage, 198, 255-270 (2019).

[14]   Goodfellow, I., Pouget-Abadie, J., Mirza, M., Xu, B., Warde-Farley, D., Ozair, S., ... & Bengio, Y., "Generative adversarial nets", Advances in neural information processing systems, 27 (2014).

[15]   Xia, T., Chartsias, A., Wang, C., Tsaftaris, S. A., & Alzheimer's Disease Neuroimaging Initiative., "Learning to synthesise the ageing brain without longitudinal data", Medical Image Analysis, 73, 102169 (2021).

[16]   Huang, X., Liu, M. Y., Belongie, S., & Kautz, J., "Multimodal unsupervised image-to-image translation", In Proceedings of ECCV, pp. 172-189 (2018).

[17]   Dewey, B. E., Zuo, L., Carass, A., He, Y., Liu, Y., Mowry, E. M., ... & Prince, J. L., "A disentangled latent space for cross-site MRI harmonization", In MICCAI, pp. 720-729 (2020).

[18]   Liu, M., Maiti, P., Thomopoulos, S., Zhu, A., Chai, Y., Kim, H., & Jahanshad, N., "Style transfer using generative adversarial networks for multi-site mri harmonization", In MICCAI, pp. 313-322 (2021).

[19]   Jiang, J., & Veeraraghavan, H., "Unified cross-modality feature disentangler for unsupervised multi-domain MRI abdomen organs segmentation", In MICCAI, pp. 347-358 (2020).

[20]   Choi, Y., Uh, Y., Yoo, J., & Ha, J. W., "Stargan v2: Diverse image synthesis for multiple domains", CVPR, pp. 8188-8197 (2020).

[21]   Karras, T., Laine, S., & Aila, T., "A style-based generator architecture for generative adversarial networks", In CVPR, pp. 4401-4410 (2019).

[22]   Huang, X., & Belongie, S., "Arbitrary style transfer in real-time with adaptive instance normalization", In Proceedings ICCV, pp. 1501-1510 (2017).

[23]   Zhao, F., Wu, Z., Wang, L., Lin, W., Xia, S., Shen, D., ...& UNC/UMN Baby Connectome Project Consortium, "Harmonization of infant cortical thickness using surface-to-surface cycle-consistent adversarial networks", MICCAI, pp. 475-483 (2019).

[24]   Wang, X., Yu, K., Wu, S., Gu, J., Liu, Y., Dong, C., ... & Change Loy, C., "Esrgan: Enhanced super-resolution generative adversarial networks", In Proceedings ECCV workshops, pp. 0-0 (2018).

[25]   Miller, K. L., Alfaro-Almagro, F., Bangerter, N. K., Thomas, D. L., Yacoub, E., Xu, J., ... & Smith, S. M., "Multimodal population brain imaging in the UK Biobank prospective epidemiological study", Nature neuroscience, 19(11), 1523-1536 (2016).

[26]   Isensee, F., Schell, M., Pflueger, I., Brugnara, G., Bonekamp, D., Neuberger, U., ... & Kickingereder, P., "Automated brain extraction of multisequence MRI using artificial neural networks", OHBM, 40(17), 4952-4964 (2019).

[27]   Jenkinson, M., Bannister, P., Brady, M., & Smith, S., "Improved optimization for the robust and accurate linear registration and motion correction of brain images", Neuroimage, 17(2), 825-841 (2002).

[28]   Tremblay-Mercier, J., Madjar, C., Das, S., Binette, A. P., Dyke, S. O., Étienne, P., ... & PREVENT-AD Research Group., "Open science datasets from PREVENT-AD, a longitudinal cohort of pre-symptomatic Alzheimer's disease", NeuroImage: Clinical, 31, 102733 (2021).

[29]   Breitner, J. C. S., Poirier, J., Etienne, P. E., & Leoutsakos, J. M., "Rationale and Structure for a New Center for Studies on Prevention of Alzheimer's Disease (StoP-AD)", The journal of prevention of Alzheimer's disease, 3(4), 236-242 (2016).

[30]   Zhang, Y., Brady, M., & Smith, S., "Segmentation of brain MR images through a hidden Markov random field model and the expectation-maximization algorithm", IEEE transactions on medical imaging, 20(1), 45-57 (2001).

[31]   Thyreau, B., Sato, K., Fukuda, H., & Taki, Y., "Segmentation of the hippocampus by transferring algorithmic knowledge for large cohort processing", Medical image analysis, 43, 214-228 (2018)

[32]   Zhang, Z., Song, Y. and Qi, H., "Age progression/regression by conditional adversarial autoencoder", In CVPR, pp. 5810-5818 (2017).

[33]   Kwon, G., Chihye H., and Dae-shik K., "Generation of 3D brain MRI using auto-encoding generative adversarial networks" In MICCAI, pp. 118-126 (2019).